ISBN: 978-3-95450-234-9 ISSN: 2673-5504 doi:10.18429/JACoW-SRF2023-WEPWB113

EVALUATION OF PHOTO-CATHODE PORT MULTIPACTING IN THE SRF PHOTO-INJECTOR CRYOMODULE FOR THE LCLS-II HIGH-ENERGY UPGRADE*

Z. Yin†, W. Hartung, S. Kim, T. Konomi, T. Xu
Facility for Rare Isotope Beams, Michigan State University, East Lansing, MI, USA

Abstract

The high-energy upgrade of the Linac Coherent Light Source will increase the photon energy and brightness. A low-emittance injector (LEI) was proposed to increase the photon flux for high X-ray energies. FRIB, HZDR, Argonne, and SLAC are developing a 185.7 MHz superconducting radio-frequency photo-injector cryomodule for the LEI. The photo-cathode system requirements are challenging, as cathodes must be maintained at the desired temperature, precisely aligned, and operated without multipacting (MP); to avoid field emission, cathode exchange must be particulate-free. A support stalk has been designed to hold the cathode in position under these requirements. A DC bias is used to inhibit MP. We simulated MP for various surface conditions and bias levels. An RF/DC test was developed to evaluate the cathode stalk performance as a subsystem and to identify and correct issues before assembly into the full cryomodule. The RF/DC test makes use of a resonant coaxial line to generate an RF magnetic field similar to that of the cathode-in-SRF-PI-cavity case. High-power test results will be presented and compared to the MP simulations.

INTRODUCTION

The Linac Coherent Light Source (LCLS-II) [1] has been a pioneering facility in the field of X-ray free-electron lasers (XFELs), providing invaluable insights into various scientific disciplines. To further advance the capabilities of LCLS-II and increase the photon energy and brightness, a high-energy upgrade known as LCLS-II-HE is underway. The low-emittance injector (LEI), which aims to enhance the photon flux for high X-ray energies, was proposed. As part of this effort, a collaboration between FRIB, HZDR, Argonne, and SLAC has focused on the development of a 185.7 MHz superconducting radio-frequency photo-injector (SRF-PI) cryomodule for the LEI [2, 3]. A novel support stalk has been designed to securely hold the cathode in position while meeting the stringent requirements of the SRF-PI [4]. This support stalk plays a crucial role in maintaining the desired temperature of the cathode, achieving precise alignment, and inhibiting multipacting (MP)—an important resonance process that can lead to detrimental effects such as elevated temperature and vacuum pressure, thereby impacting photocathode stability and lifetime. To address this, a DC bias is applied.

* Work supported by the Department of Energy Contract DE-AC02-76SF00515
† yin@frib.msu.edu

To evaluate the performance of the cathode stalk as a subsystem and identify any issues before assembly into the full cryomodule, an RF/DC test has been developed as shown in Fig. 1. This test utilizes a resonant coaxial line to generate an RF magnetic field that closely resembles the conditions inside the cathode-in-SRF-PI-cavity case. The desired magnitude of the accelerating field at the photocathode is set at 30MV/m. In this paper, we compare the results obtained from the RF/DC test with MP simulations conducted for various surface conditions and bias levels.

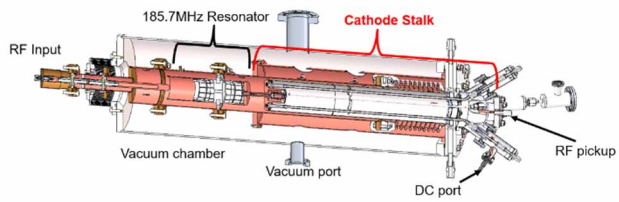

Figure 1: Setup for RF/DC test [4].

MULTIPACTING SIMULATION

CST Microwave Studio (CST) was utilized to conduct simulations of the MP process, and the simulated structure is presented in Fig. 2. To be analogous to real-world scenarios involving cosmic rays, photoemission, or impacting field emissions, initial particles were distributed in a Gaussian manner over time, with a bunch length corresponding to the RF (radio frequency) period. The occurrence of MP in RF structures relies on both the electromagnetic field distribution and the secondary emission yield (SEY) of the materials [5]. We use CST to generate the distributions of RF and DC fields, which were subsequently employed as inputs for the particle simulation. The resulting RF field maps are presented in Fig. 3. Within the cathode stalk, multiple materials were utilized, and their typical SEY values were employed for simulation purposes. The SEY curves for various materials can be observed in Fig. 4 [6-9]. To examine the influence of DC bias and surface conditions, we initially simulated MP without any DC bias and subsequently varied the DC bias to demonstrate its suppressive effect. Additionally, we explored different surface conditions by modifying the SEY values of the various materials.

Without DC Bias

Initially, the simulation is conducted in the absence of DC bias, while altering the RF field distribution. The adjustments made to the field distribution within the cathode

ISBN: 978-3-95450-234-9 ISSN: 2673-5504 doi:10.18429/JACoW-SRF2023-WEPWB113

stalk of the experimental setup correspond to the actual operational scenario of the cathode-in-SRF-PI-cavity, where the gradient at the photocathode ranges from 2 MV/m to 30 MV/m. The initial particle sources are positioned on the various surfaces within the structure, as illustrated in Fig. 2. These sources are divided into four distinct regions for analysis: Region I corresponds to the area surrounding the Fundamental Power Coupler (FPC) and dummy resonator; Region II represents the region between the outer wall of the stalk and the inner wall of the outer structure; Region

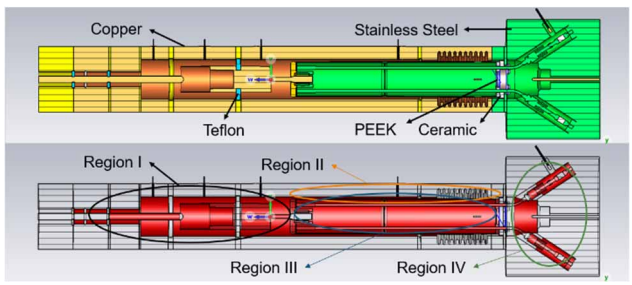

Figure 2: Simulation module of cathode stalk and initial particle source distribution.

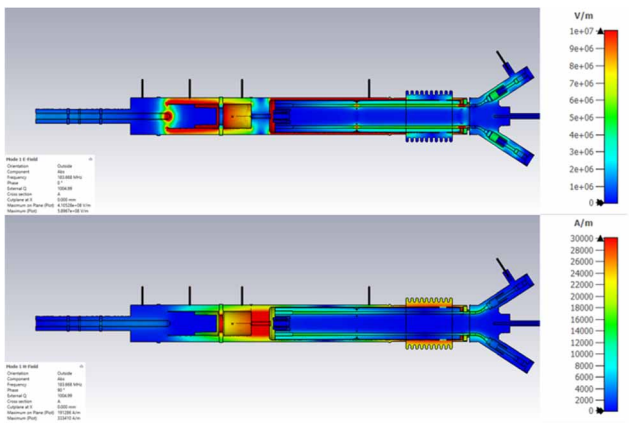

Figure 3: Electric filed (above) and magnetic field (blow) distribution maps when total energy of electromagnetic field is 1 J.

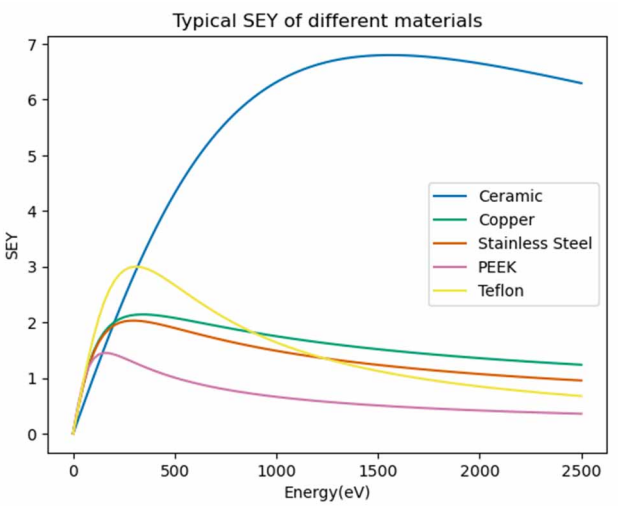

Figure 4: Typical SEY of different materials.

III denotes the interior area of the stalk; and Region IV encompasses the vicinity around the cooling tube situated outside the stalk.

In general, the number of electrons exhibits an exponential increase when the space charge effect is not taken into account. The growth rate, defined as the coefficient of the exponent, varies with different electric field at the photocathode. The representation of these growth rates is depicted in Fig 5. Fig. 6 displays the electron distributions subsequent to the occurrence of MP within each respective region. Furthermore, the CST 3D particle position monitor provides a clear depiction of the resonant behavior of electrons between adjacent walls. Within Region III, the electrons exhibit a bidirectional motion along the cylindrical tube, wherein a fraction of electrons collide with the cooling tubes and subsequently retreat in their trajectory. Based on the simulation results, it can be deduced that in the absence of DC bias, when the cathode gradient remains below 30 MV/m, MP manifests in Region II at low gradients and in Region IV at high gradients. Besides, it is observed that MP activity is relatively weak in Region I and even more subdued in Region III.

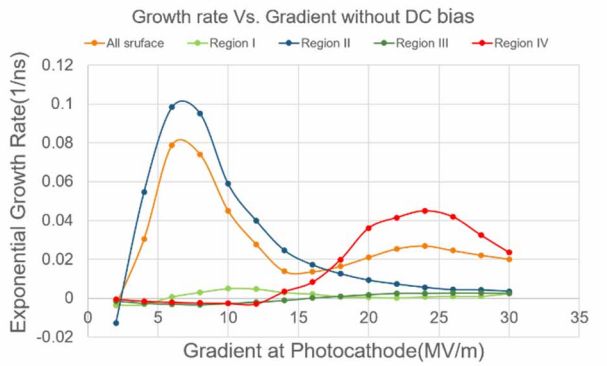

Figure 5: Growth rate versus field gradient for different region of initial particle source.

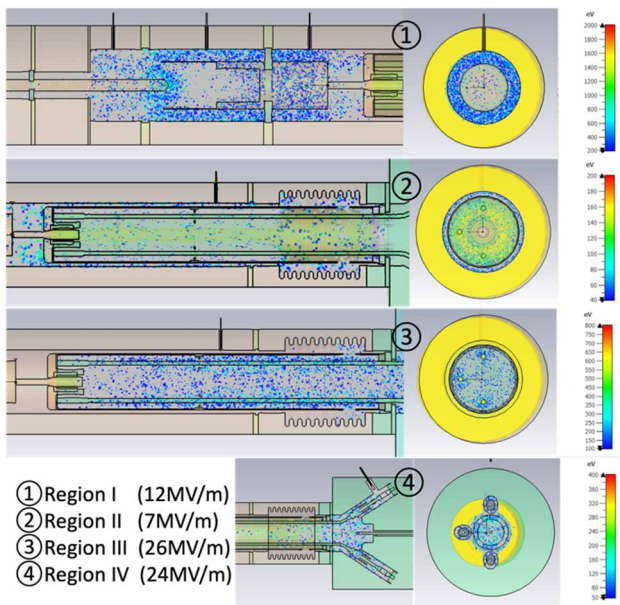

Figure 6: Electron distribution at different region after MP.

ISBN: 978-3-95450-234-9 ISSN: 2673-5504 doi:10.18429/JACoW-SRF2023-WEPWB113

Various DC Bias Levels

Subsequently, various DC bias levels are introduced to investigate the threshold field gradient at which (MP) initiation occurs, characterized by a growth rate surpassing zero. The simulations encompass all four regions, and the corresponding outcomes are illustrated in Fig. 7. Remarkably, the application of DC bias proves to be highly effective in suppressing MP, as the threshold gradient exceeds 30 MV/m when the magnitude of the DC bias exceeds approximately 600 V. Notably, negative bias exhibits superior suppression capabilities. Regions II and IV, which were previously identified as harbouring stronger instances of MP, experience greater inhibition compared to the other two regions. Region III, specifically, exhibits enhanced suppression with negative bias, while positive bias demonstrates improved inhibition within Region IV, as negative bias serves to expel electrons from Region III and vice versa.

Various Surface Conditions

In this particular case, a constant DC bias of -1 kV is maintained, successfully mitigating MP based on the aforementioned simulation results. Considering that materials can exhibit varying secondary emission yields (SEY) before and after specific operations such as baking and RF processing, we proceed to modify the SEY values of the key materials constituting this structure and compare the simulation outcomes. Specifically, copper and stainless steel, which are prone to experiencing MP in the absence of DC bias, have their SEY values adjusted and are subsequently subjected to simulation. Additionally, we investigate the effects of altering the SEY values of ceramic, Teflon, and PEEK. Ultimately, no modifications are made due to the observed increase in the SEY values of the different materials.

Summary

Based on the simulation results, it is observed that MP occurs in various regions within the structure under investigation. Nevertheless, it is noteworthy that all instances of MP can be effectively suppressed and exhibit no correlation with the SEY of the materials when a DC bias of -1 kV is applied. This finding highlights the significant influence of the DC bias in mitigating MP, suggesting a strong dependence between MP occurrence and the applied DC bias.

MEASUREMENT COMPARISON

The configuration for the RF/DC setup employed in the cathode stalk experiment is depicted in Fig. 1. The comprehensive results of the RF/DC test can be found in the corresponding reference [10]. In order to detect the occurrence of MP, two resistances are connected to the high voltage wire and the FPC wire, facilitating the measurement of current and serving as indicators for the presence of MP. The pressure level within the system is also utilized as an additional indicator. To determine the threshold electric field at each voltage, various bias voltages were employed, and the input power was systematically increased. These measurements were performed at room temperature. The obtained results are presented in Fig. 8, alongside the corresponding simulation outcomes, providing a comprehensive basis for comparison and analysis. At DC bias magnitudes below 500 V, only the FPC current was detected. However, when the voltage exceeded 500 V, only the cathode current was detected, indicating a transition in the location of MP. Subsequently, a processing procedure was carried out by progressively increasing the duty factor of the pulsed RF field at maximum input power. Notably, even when the input power reached its maximum value, resulting in an electric field of approximately 44 MV/m at the photocathode after processing, no instances of MP were observed.

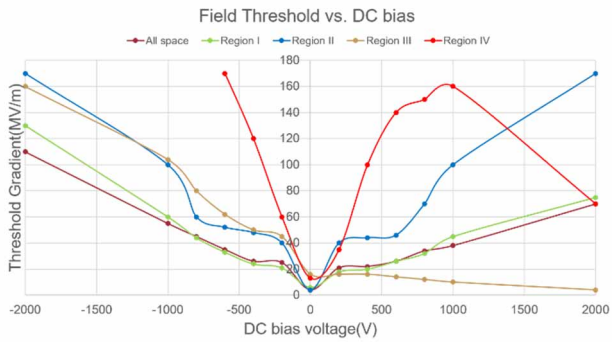

Figure 7: MP threshold versus DC bias from simulation for various regions.

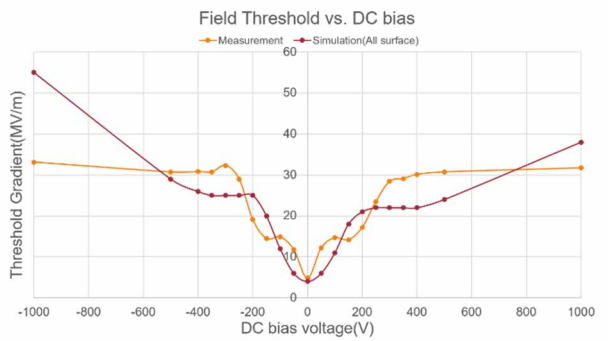

Figure 8: MP threshold versus DC bias from measurement and simulation.

One notable disparity between the simulation and experimental results is the saturation of the MP threshold at around 30MV/m observed in the measurements when the magnitude of the DC bias exceeded approximately 400 V. In contrast, the simulation results continued to exhibit an increasing trend. Moreover, it was observed that MP occurrence in each region was influenced by the applied DC bias, even in Region III where the electric field generated by the DC bias was relatively small. Interestingly, the experimental findings indicated the presence of MP in certain unexpected regions, independent of the effects of DC bias. The identification of different current types detected in the experimental measurements provides an explanation for the occurrence of MP in Region I at low DC bias, consistent with the simulation results. However, it should be

ISBN: 978-3-95450-234-9 ISSN: 2673-5504 doi:10.18429/JACoW-SRF2023-WEPWB113

noted that at high DC bias levels, MP was detected at certain locations not previously identified in the simulation results.

SUMMARY

The numerical simulation of MP by CST in the cathode stalk reveals a pronounced correlation between the threshold gradient and the applied DC bias, with a noteworthy observation that a -1 kV bias effectively suppresses MP when the electric field at the photocathode reaches 30 MV/m. However, experimental measurements demonstrate that the MP threshold gradient saturates at 30 MV/m for DC bias levels exceeding 400 V. This suggests the occurrence of MP at certain locations that were not captured in the simulation analysis.

OUTLOOK

Due to the complexity of the cathode stalk structure, the specific position of MP was not identified for the -1 kV DC bias, necessitating further in-depth research. There are several factors of concern in this regard. Firstly, the distribution of RF fields, which plays a significant role in the MP process, may differ slightly when minor modifications are made to the module. For instance, in the simulation module, the high voltage wire was not included. Secondly, there is a possibility that the mesh density may be insufficient in certain locations, warranting an increase in the mesh resolution at positions where the DC field nearly diminishes based on the measurement results. Additionally, to enhance the robustness of our findings, we plan to conduct repetitive measurements at both room temperature and liquid nitrogen temperature subsequent to rinsing and baking the test setup.

REFERENCE

[1] J. Stohr, "Linac Coherent Light Source II (LCLS-II) Conceptual Design Report", United States, 2011. doi:10.2172/1029479

[2] J.W. Lewellen *et al.*, "Status of the SLAC/MSU SRF Gun Development Project", *in Proc. NAPAC'22*, Albuquerque, NM, USA, Aug. 2022, pp. 623-626. doi:10.18429/JACoW-NAPAC2022-WEPA03

[3] S.H. Kim *et al.*, "Design of a 185.7 MHz Superconducting RF Photoinjector Quarter-Wave Resonator for the LCLS-II-HE Low Emittance Injector", in *Proc. NAPAC'22*, Albuquerque, NM, USA, Aug. 2022, pp. 245-248. doi:10.18429/JACoW-NAPAC2022-MOPA85

[4] T. Konomi *et al.*, "Design of the Cathode Stalk for the LCLS-II-HE Low Emittance Injector", in *Proc. NAPAC'22*, Albuquerque, NM, USA, Aug. 2022, pp. 253-255. doi:10.18429/JACoW-NAPAC2022-MOPA87

[5] H. Padamsee, J. Knobloch, and T. Hays, "Multipacting", in *RF Superconductivity for Accelerators*, Wiley-VCH Verlag GmbH &Co. KGaA, Weinheim, pp. 179–198, 2008.

[6] Suharyanto, S. Michizono, Y. Saito, Y. Yamano, and S. Kobayashi, "Secondary electron emission of TiN-coated alumina ceramics", *Vacuum*, vol. 81(6), pp. 799–802, 2007. doi:10.1016/j.vacuum.2005.11.062

[7] V. Baglin *et al.*, "The Secondary Electron Yield of Technical Materials and its Variaton with Surface Treatments", in *Proc. EPAC'00*, Vienna, Austria, Jun. 2000, paper THXF102, pp. 217-221. https://jacow.org/e00/papers/THXF102.pdf

[8] Y. Chen, J. Wu, M. Cho, and K. Toyoda, "Total electron emission yields of typical polymers", 2013 IEEE International Conference on Solid Dielectrics (ICSD), Bologna, Italy, pp. 752–755, 2013. doi:10.1109/ICSD.2013.6619757

[9] R.F. Willis and D.K. Skinner, "Secondary electron emission yield behaviour of polymers", *Solid State Commun.*, 13(6), pp. 685–688, 1973. doi:10.1016/0038-1098(73)90459-6

[10] T. Konomi *et al.*, "Design and Tests of a Cathode Stalk for the LCLS-II-HE Low Emittance Injector SRF Gun", presented at the SRF'23, Grand Rapids, MI, USA, Jun. 2023, paper TUPTB069, this conference.